OPTICAL STOCHASTIC COOLING AT IOTA RING*

V. A. Lebedev# and A. L. Romanov, FNAL, Batavia, IL 60510, USA

Abstract

The optical stochastic cooling (OSC) represents a promising novel technology capable to achieve fast cooling rates required to support high luminosity of future hadron colliders. The OSC is based on the same principles as the normal microwave stochastic cooling but uses much smaller wave length resulting in a possibility of cooling of very dense bunches. In this paper we consider basic principles of the OSC operation and main limitations on its practical implementation. Conclusions will be illustrated by Fermilab proposal of the OSC test in the IOTA ring.

INTRODUCTION

The stochastic cooling [1 - 4] has been successfully used in a number of machines for particle cooling and accumulation. Cooling rates of few hours required for luminosity control in hadron colliders cannot be achieved in the microwave frequency range (~10^9-10^{10} Hz) usually used in stochastic cooling. Large longitudinal particle density used in such colliders requires an increase of cooling bandwidth by few orders of magnitude. To achieve such increase one needs to make a transition to much higher frequencies. A practical scheme operating in the optical frequency range was suggested in Ref. [5]. The method is named the optical stochastic cooling (OSC). It is based on the same principles as the stochastic cooling but uses much higher frequencies. Consequently, it is expected to have a bandwidth of ~10^{13}–10^{14}Hz and can create a way to attain required cooling rates.

Fermilab plans to make an experimental test of the OSC in IOTA ring [6]. Details of the project have been changing with improved understanding of the experiment. In particular, the basic wave length of the wiggler radiation was changed from 0.8 to 2.2 μm to achieve reasonably large cooling and dynamic apertures. The reasons of this transition will be discussed in the following sections.

In the OSC a particle emits e.-m. radiation in the first (pickup) wiggler. Then, the radiation amplified in an optical amplifier (OA) makes a longitudinal kick to the same particle in the second (kicker) wiggler as shown in Figure 1. A magnetic chicane is used to make space for the OA and to delay a particle so that to compensate for a delay of its radiation in the OA resulting in simultaneous arrival of the particle and its amplified radiation to the kicker wiggler. A particle passage through the chicane has a coordinate-dependent correction of particle longitudinal position which, consequently, results in a correction of relative particle momentum, $\delta p/p$, with amplitude ξ_0 so that:

$$\delta p / p = -\xi_0 \sin\left(k\,\Delta s\right) . \qquad (1)$$

Here $k = 2\pi/\lambda$ is the radiation wave-number,

$$\Delta s = M_{51}x + M_{52}\theta_x + M_{56}\left(\Delta p / p\right) \qquad (2)$$

is the particle displacement on the way from pickup to kicker relative to the reference particle which experiences zero displacement and obtains zero kick, M_{5n} are the elements of 6x6 transfer matrix from pickup to kicker, x, θ_x and $\Delta p/p$ are the particle coordinate, angle and relative momentum deviation in the pickup.

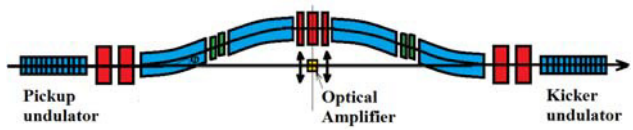

Figure 1: OSC schematic; blue – dipoles, red quadrupoles, green - sextupoles.

For small amplitude oscillations the horizontal and vertical cooling rates per turn are [7]:

$$\begin{bmatrix}\lambda_x\\ \lambda_s\end{bmatrix} = \frac{k\xi_0}{2}\begin{bmatrix}M_{56}-S_p\\ S_p\end{bmatrix}, \qquad (3)$$

where $S_p = M_{51}D_p + M_{52}D'_p + M_{56}$ is the partial slip-factor introduced so that for a particle without betatron oscillations and with momentum deviation $\Delta p/p$ the longitudinal displacement relative to the reference particle on the way from pickup to kicker is equal to $S_p\Delta p/p$, and D_p and D'_p are the dispersion and its derivative in the pickup. Eq. (3) assumes an absence of x-y coupling in the chicane. Introduction of x-y coupling outside the cooling area redistributes the horizontal cooling rate between two transverse planes but does not change the sum of cooling rates which is equal to: $\Sigma\lambda_n = k\xi_0 M_{56}/2$, $n = x, y, s$.

Although M_{56} and, consequently, the sum of cooling rates depend only on focusing inside the chicane, S_p and the ratio of cooling rates depend on the dispersion at the chicane beginning, *i.e.* on the ring dispersion. Eq. (3) yields the ratio of cooling rates:

$$\lambda_x / \lambda_s = M_{56} / S_p - 1 . \qquad (4)$$

A non-linear dependence of kick on Δs in Eq. (1) results in a dependence of cooling rates on amplitudes [7]:

$$\begin{aligned}\lambda_x(a_x,a_s) &= \left(2\,\mathrm{J}_0(a_s)\,\mathrm{J}_1(a_x)/a_x\right)\lambda_x \quad ,\\ \lambda_s(a_x,a_s) &= \left(2\,\mathrm{J}_0(a_x)\,\mathrm{J}_1(a_s)/a_s\right)\lambda_s \quad ,\end{aligned} \qquad (5)$$

where a_x and a_s are the amplitudes of longitudinal particle displacement relative to the reference particle on the way from pickup to kicker due to betatron and synchrotron oscillations expressed in the units of e.-m. wave phase:

$$\begin{aligned}a_x &= k\sqrt{\varepsilon_1\left(\beta_p M_{51}^{\,2} - 2\alpha_p M_{51}M_{52} + \left(1+\alpha_p^{\,2}\right)M_{52}^{\,2}\right)},\\ a_p &= k\left|S_p\right|\left(\Delta p / p\right) \quad ,\end{aligned} \qquad (6)$$

ε_1 is the Courant-Snyder invariant of a particle, β_p and α_p are the horizontal beta-function and its negative half derivative in the pickup, and $(\Delta p/p)$ is the amplitude of particle synchrotron motion. As one can see from Eqs. (5) each cooling rate changes its sign if any of amplitudes

*Work supported by Fermi Research Alliance, LLC, under Contract No. DE-AC02-07CH11359 with the United States Dep. of Energy
#val@fnal.gov

ISBN 978-3-95450-174-8

exceeds the first root, μ_{01}, of the Bessel function $J_0(x)$. Thus the cooling area is bounded by $a_x=\mu_{01}$ and $a_y=\mu_{01}$ where $\mu_{01}\approx 2.405$. Using Eqs. (6) one obtains from these equations the cooling area boundaries:

$$\varepsilon_{\max} = \frac{{\mu_{01}}^2}{k^2\left(\beta_p {M_{51}}^2 - 2\alpha_p M_{51}M_{52} + \left(1+{\alpha_p}^2\right){M_{52}}^2\right)}, \quad (7)$$

$$\left(\Delta p / p\right)_{\max} = \mu_{01}\Big/\left(k\left|S_p\right|\right) \ .$$

As one can see the cooling boundary for betatron motion does not depend on the ring dispersion in the OSC area but depends on the ring horizontal beta-function.

BEAM OPTICS OF OSC INSERT

The IOTA ring is a dual purpose storage ring aimed at experiments in the integrable optics [8, 9] and the OSC. Normally the machine is expected to operate with electrons up to 150 MeV kinetic energy. Operation with 2.5 MeV protons (~70 MeV/c momentum) is also anticipated in the program of integrable optics studies.

The energy for the OSC test is chosen to be 100 MeV [6]. The OSC system will take one of four ring straight sections with total length of about 4.5 m. The main parameters of the IOTA ring operating with OSC are shown in Table 1. It is implied that the rms horizontal emittance and momentum spread are determined by synchrotron radiation (SR) and *x-y* coupling is absent.

Table 1: Main Parameters of IOTA Storage Ring for OSC

Circumference	40 m
Nominal beam energy	100 MeV
Bending field	4.8 kG
Tunes, Q_x/Q_y	5.45/3.45
Rms hor. emittance, ε (no *x-y* coupling)	9.1 nm
Rms momentum spread, σ_p	$1.07\cdot10^{-4}$
SR cooling rates (ampl.), $\lambda_x=\lambda_y/\lambda_s$, s^{-1}	0.54/0.92

The cooling chicane consists of four dipoles with parallel edges (Figure 1). In the absence of additional focusing inside the chicane M_{56} and S_p are equal and horizontal OSC is absent. An introduction of quadrupole focusing in the chicane center makes M_{56} and S_p different and, consequently, creates transverse cooling. To understand interdependencies between major parameters we use a thin lens approximation. Leaving only leading terms one obtains the following estimates for elements of kicker-to-pickup transfer matrix:

$$M_{51}=M_{26}\approx -\Phi h\ ,\ M_{52}=M_{16}\approx -\Phi h L_{tot}\ ,\ M_{56}\approx 2\Delta L\ . \quad (8)$$

That results in $S_p \approx 2\Delta L - \Phi D^* h$. Here ΔL and h are the path lengthening and the trajectory offset in the chicane, $\Phi \equiv -1/F$ is the defocusing strength of the quad, and L_{tot} is the half-length of the chicane (distance from its center to the outer edge of outer dipole). Assuming $dD/ds=0$ in the chicane center and neglecting dispersion changes in the chicane one obtains from Eq. (4):

$$R_c \equiv \lambda_x/\lambda_s \approx \Phi D^* h \Big/ \left(2\Delta L - \Phi D^* h\right)\ , \quad (9)$$

where is D^* is the dispersion in the chicane center. Note that the above requirement of $dD/ds=0$ minimizes the equilibrium beam emittance set by SR. As one can see from Eq. (9) $\Phi D^* h/\Delta L$ uniquely determines the ratio of cooling rates.

Similarly, using Eqs. (7) and (9) one obtains estimates for the cooling area boundaries:

$$\left(\frac{\Delta p}{p}\right)_{\max} \approx \frac{\mu_{01}}{\left(2\Delta s - \Phi D^* h\right)k} = \frac{\mu_{01}\left(1+R_c\right)}{2k\Delta L}\ , \quad (10)$$

$$\varepsilon_{\max} \approx \frac{{\mu_{01}}^2}{k^2 h^2 \Phi^2 \beta^*} \approx \frac{{\mu_{01}}^2 {D^*}^2}{4\Delta L^2 k^2 \beta^*}\left(\frac{1+R_c}{R_c}\right)^2\ , \quad (11)$$

where $\beta^* \approx L^2/\beta$ is the beta-function in the chicane center, and we took into account that $\varepsilon_{\max}$ achieves maximum when $d\beta/ds=0$ in the chicane center. One can see that the cooling acceptance, $\varepsilon_{\max}$, is inversely proportional to β^*, which in the case of IOTA results in a collider type optics in the cooling area with minimum of horizontal beta-function in the chicane center. The value of ΔL is determined by a delay in the OA and has been chosen to be 3 mm. As one can see from Eqs. (10) and (11) an increase of R_c results in an increase of longitudinal cooling acceptance but reduces the transverse one.

Non-linear contributions to the longitudinal particle displacement omitted in Eq. (2) represent another important limitation on the cooling chicane parameters. These contributions are dominated by path lengthening due to betatron motion on the travel from pickup to kicker. In the case of small β^* in the chicane center one obtains that the non-linear path lengthening oscillates with betatron phase and at maximum the second order contribution is estimated as [7]:

$$\Delta s_2 \approx -\frac{1}{2}\int \theta(s)^2 ds \approx -\frac{\varepsilon_1}{\beta^*} L_{tot}\ . \quad (12)$$

Table 2: Optics Structure for Half of OSC Insert

	Length [cm]	B/G/S
Chicane center	-	-
D quad (half)	3	-86 G/cm
Drift	5	
F quad	6	0
Drift	7	
Dipole	8	-3060 G
Drift	10	
D sextupole	10	-830 G/cm^2
Drift	11	
F sextupole	10	1550 G/cm^2
Drift	10	
Dipole	8	3060 G

One can see that Δs_2 is proportional to the particle Courant-Snyder invariant and is inversely proportional to the beta-function in the chicane center. That yields that the 2-nd order contribution due to horizontal betatron motion will be much larger than due to vertical motion. Two pairs of sextupoles located between each couple of chicane dipoles (see Figure 1 and Table 2) are added for non-linear lengthening compensation.

The above estimates were directing the choice of chi-

ISBN 978-3-95450-174-8

cane parameters. After a few iterations we came to a reasonable compromise between contradictory requirements. Tables 2 and 3 present parameters of the OSC insert structure and the major parameters of OSC optics. Figure 2 shows the beta-functions and dispersion in the OSC straight. The cooling ranges in Table 3 are determined as ratio of cooling boundaries of Eq. (7) to the rms horizontal emittance set by SR in absence of coupling or the rms momentum spread: $n_{\sigma x}=\varepsilon_{max}/\varepsilon$, $n_{\sigma s}=(\Delta p/p)_{max}/\sigma_p$.

Table 3: Major Parameters of OSC Optics

Delay in the chicane, Δs	3 mm
Horizontal beam offset, h	43 mm
M_{56}	5.81 mm
Dispersion in the chicane center, D^*	600 mm
Beta-function in the chicane center, β^*	52 mm
Cooling rates ratio, λ_x/λ_s (no x-y coupl.)	1.7
Cooling ranges (before OSC), $n_{\sigma x}/n_{\sigma s}$	5.9 / 3.7

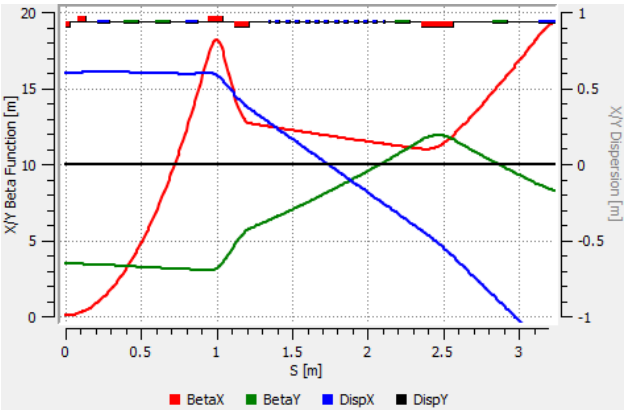

Figure 2: The beta-functions and dispersion in the half of OSC straight (from the chicane center to the first dipole).

To compute the longitudinal particle displacement on the way from pickup to kicker, Δs, we considered idealized model which has ideal rectangular dipoles with rigid edges and point-like sextupoles. Particle motion inside dipole was described by a piece of spiral to account for the vertical betatron motion. Vertical focusing of the dipole edges due to finite gap in the dipoles was accounted. As it was expected, in the absence of sextupole compensation the longitudinal particle displacement is dominated by the non-linear contribution coming from the betatron motion. As can be seen in Figure 3 that results in a significant reduction of the cooling boundaries - to about 1.5 and 5σ for the horizontal and vertical betatron motions, respectively. The sextupole compensation greatly reduces the non-linearities and increases the cooling boundaries to about 5σ and 7σ. Note that in the absence of nonlinearities the curves shown in Figure 3 would represent concentric ellipses required for OSC. Computations show that non-linearity in the longitudinal degree of freedom is negligible. Note also that Eq. (12) underestimates non-linear contribution to particle displacement by about 50%.

The sextupoles in the OSC straight introduce considerable nonlinearity to the betatron motion. Figure 4 presents distortion of constant action ellipses after passing the OSC chicane. As one can see the distortions are well visible for 4σ ellipse in the horizontal plane but hardly visible for the vertical plane even for 8σ amplitudes.

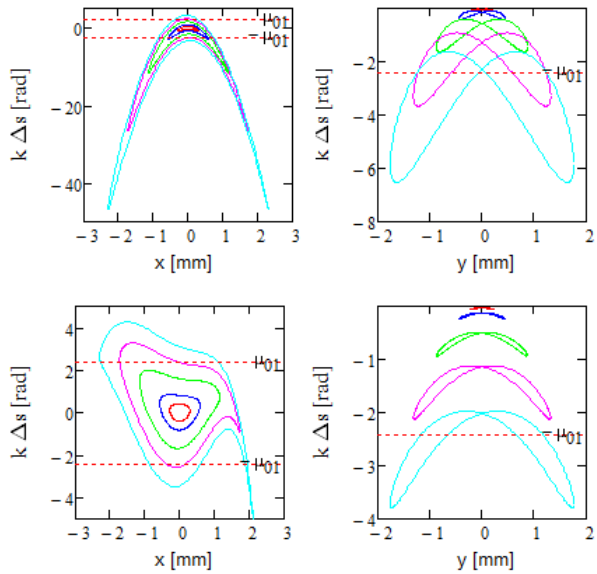

Figure 3: Dependence of the normalized longitudinal particle displacement in the kicker, $k\Delta s$, on the transverse particle position in the pickup for particles located at ellipses of 1σ, 2σ, 4σ, 6σ and 8σ; left and right - horizontal and vertical betatron motions, respectively; bottom and top - with and without sextupole correction, respectively. Amplitudes of betatron motion are referenced to the equilibrium horizontal emittance, ε, in the absence of x-y coupling. Horizontal lines mark cooling boundaries.

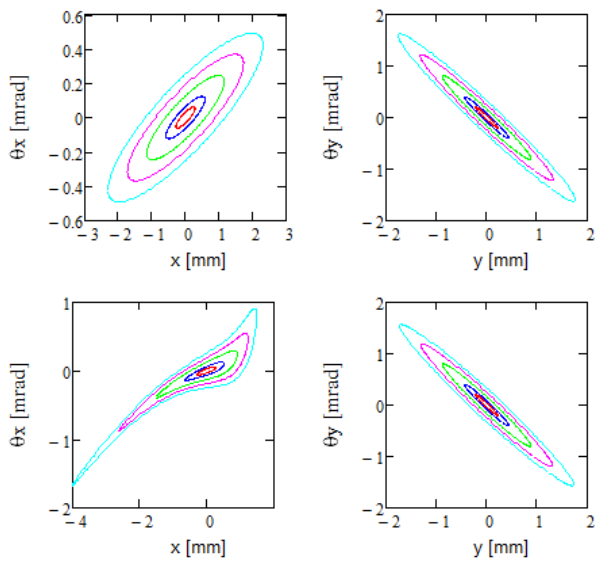

Figure 4: Horizontal (left) and vertical (right) phase spaces after coming through the chicane with (bottom) and without (top) sextupole correction. Initially particles were located at ellipses of 1σ, 2σ, 4σ, 6σ and 8σ in x or y plane.

The ring optics is symmetric relative to the chicane center. Figure 5 presents the dispersion and beta-functions for half of the ring. The optics was designed to minimize

ISBN 978-3-95450-174-8

the equilibrium emittance. It required minimization of the dispersion invariant, $A = \left(1+\alpha^2\right)D^2/\beta + 2\alpha DD' + \beta D'^2$, in the dipoles. Rewriting Eq. (11) in the following form,

$$A^* \equiv \frac{D^{*2}}{\beta^*} \approx \frac{4\varepsilon_{\max} k^2 \Delta s^2}{\mu_{01}^2}\left(\frac{R_c}{1+R_c}\right)^2, \qquad (13)$$

one can see that the dispersion invariant in the OSC chicane is determined by the ratio of cooling rates and weakly depends on other details of OSC optics. For the considered above OSC proposal the value of invariant in the OSC chicane is 6.8 m. It greatly exceeds its natural value in the IOTA ring. An adjustment of focusing for quads adjacent to the both sides of the chicane results in a reduction of the invariant after the first dipole by about two orders of magnitude. The invariant value stays at this small level for the rest of the ring. This quad adjustment has been crucial to obtain tolerable transverse emittances.

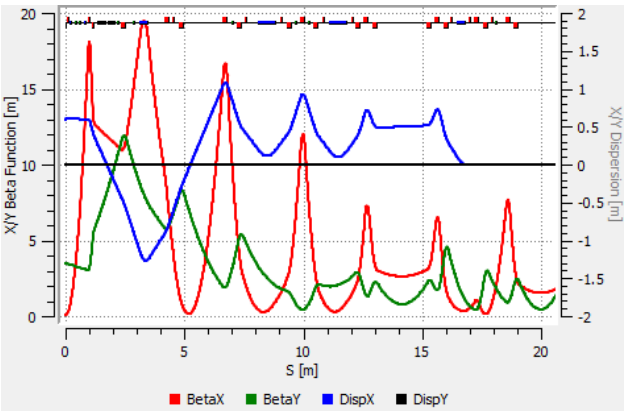

Figure 5: Optics functions for half of IOTA ring starting from the OSC section center.

Operation at the coupling resonance redistributes the SR and OSC cooling rates between horizontal and vertical planes resulting approximately equal equilibrium transverse emittances and, consequently, twice smaller horizontal emittance.

The OSC area sextupoles increase the ring chromaticity to $pd\nu_x/dp \approx 250$, $pd\nu_y/dp \approx -70$. The chromaticities were corrected by ring sextupoles split into five families. Tracking and FMA (frequency map analysis) with both chromaticities supressed to zero exhibit the dynamic apertures of about 4σ for both transverse planes. We expect that an improvement of sextupole correction and linear optics will yield further improvement of dynamic aperture. Note that the considered above cooling boundaries and dynamic apertures were referenced to the horizontal emittance of uncoupled optics. Their values need to be increased by $\sqrt{2}$ for the coupled case.

COOLING AND BEAM PARAMETERS

Presently we consider two steps in a study of the OSC. First, we will use a passive cooling where an OA is not used and the radiation of pickup undulator is focused to the kicker undulator with lens telescope. Such arrangement should be capable to increase the SR cooling rate by about an order of magnitude. The second step implies a usage of OA which should deliver further increase of OSC rates.

The OSC rates were computed using the results of Ref. [7]. Main parameters of the passive cooling scheme are shown in Table 4. In computation of cooling rates we assumed an ideal lens with optical band 2.2 - 2.9 μm. Such bandwidth is an estimate and it not supported yet by detailed design of the lens telescope. The OSC rates in Table 5 also imply operation on the coupling resonance so that the horizontal and vertical rates are equal to about half of the horizontal rate in the absence of coupling.

For operation on coupling resonance both the *x* and *y* beam emittances are about half of the equilibrium emittance, *ε*. That determines the beam sizes in the undulators to be ~250 μm for the coupled case (see Figure 6). The diffraction limited size of particle radiation in the kicker wiggler is somewhat larger, ~350 μm (radius at half height). The reduction of cooling rate for high amplitude particles was also neglected in the cooling rate estimate.

Table 4: Main Parameters for Passive OSC

Undulator parameter, K	0.8
Undulator period	12.9 cm
Peak magnetic field	664 G
Radiation wavelength at zero angle	2.2 μm
Radiation band used for OSC	2.2 - 2.9 μm
Number of periods, *m*	6
Total undulator length, L_w	77 cm
Distance between undulator centers	3.3 m
Telescope aperture, 2*a*	13 mm
Cooling rates in amplitude (*x*=*y*/*s*)	6.3/5.2 s^{-1}

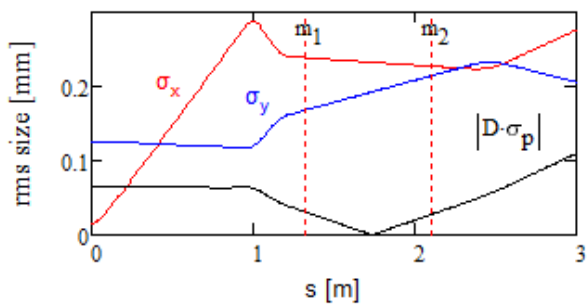

Figure 6: Rms beam sizes (vertical – σ_y, horizontal due to betatron motion – σ_x, and due to momentum spread - $|D\sigma_p|$) in the OSC region starting from the cooling chicane center. Vertical lines mark location of wiggler.

A small value of dynamic aperture greatly reduces the beam lifetime due to scattering on the residual gas. Therefore obtaining very good vacuum is a high priority task. The long term goal is $2\cdot10^{-10}$ Torr H_2 equivalent. It corresponds to 50 min. beam lifetime due to single electromagnetic scattering, and also yields that the emittance growth rate due to scattering on the residual gas is ~1% of the emittance growth rate due to quantum fluctuations of SR. The major beam and ring parameters are presented in Table 5.

ISBN 978-3-95450-174-8

The maximum number of particles per bunch is 10^6. It was chosen so that the Touschek lifetime would be longer than about 1 hour; and increases in the bunch length and horizontal emittance due to multiple IBS would not exceed 20% of their values set by the SR radiation. In computation of IBS rates we assume an operation on the coupling resonance so that $\varepsilon_x=\varepsilon_y=\varepsilon/2$ and the horizontal growth rate is equally split into x and y planes. Note also that for this small number of particles and small OSC cooling rates the cooling system operates orders of magnitude below optimal gain and the particle interaction through the OSC system can be neglected.

Table 5: Major Beam Parameters for OSC in IOTA

Geometric acceptance	5 μm
Dynamic acceptance	0.15 μm
Average vacuum (H_2 equivalent)	$2\cdot10^{-10}$ Torr
Vacuum beam lifetime	50 min.
SR losses per turn	13.3 eV
RF voltage amplitude	30 V
RF harmonic number	4
Momentum compaction	-0.0178
RF bucket height, $(\Delta p/p)_{max}$	10^{-3}
RMS bunch length (no OSC)	22 cm
Number of particles	10^6
Touschek lifetime ($\varepsilon_x=\varepsilon_y=\varepsilon/2$)	1.3 hour
Hor. emittance growth rate due to IBS	0.1 s^{-1}
Long. emittance growth time due to IBS	0.44 s^{-1}

ACTIVE AND PASSIVE OSC

In the above cooling rate estimate we assumed that the radiation emitted by a particle in the course of its motion in the pickup is focused to the location of the same particle in the kicker (when the particle arrives to it) in the course of particle entire motion in the kicker. It is automatically achieved for the lens located at the infinity (*i.e.* if the distance to the lens is much larger than the length of undulator) – the condition which is impossible to achieve in practice. A practical solution can be obtained with a lens telescope which has the transfer matrix $\mathbf{M}_T$ from the center of pickup to the center of kicker equal to $p\mathbf{I}$, where $\mathbf{I}$ is the identity matrix and $p=\pm1$. In this case the transfer matrix between emitting and receiving points is $\mathbf{O}(l)\mathbf{M}_T\,\mathbf{O}(-l)=\pm\mathbf{I}$, *i.e.* coincides with the matrix for the system where the lens is located at infinity. Here $\mathbf{O}(l)$ is the transfer matrix for a drift with length l. The simplest telescope requires 3 lenses (see Figure 7). For symmetrically located lenses there are only two possible solutions:

$$\text{(I)}\quad F_1=L_1,\quad F_2=-\frac{L_1^2}{2(L-L_1)},\quad p=-1;$$
$$\text{(II)}\quad F_1=\frac{LL_1}{L+L_1},\quad F_2=\frac{L_1^2}{2(L+L_1)},\quad p=1. \qquad (14)$$

The first solution requires weaker focusing, has smaller focusing chromaticity, and therefore is preferred. It also has defocusing lens in the center which is preferred from manufacturing point of view. The lens telescope is located inside the cooling chicane which determines its parameters: L=165 cm, $L_1=F_1=20$ cm, $F_2=-1.6$ cm. The diagonal elements of transfer matrix for the beam optics are also negative ($M_{11}=M_{22}=-1.03$, $M_{33}=M_{44}=-2.07$). It greatly mitigates the problem of cooling rate reduction for particles with large betatron amplitudes due to transverse separation of a particle and its radiation in the kicker undulator. As M_{11} and M_{22} are quite close to -1 this effect is strongly suppressed for the horizontal betatron motion.

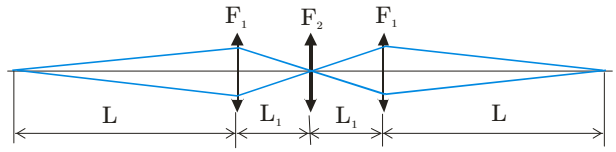

Figure 7: Light optics layout for passive cooling.

Non-linear contribution to the sample lengthening forced us to increase the base wave length for OSC test from 0.8 μm to 2.2 μm. As result we switched from the OA based on Ti: Sapphire crystal to Cr:ZnSe crystal. This crystal can support ~10% bandwidth with gain of about 10 Db. Further details can be found in Ref. [10].

CONCLUSIONS

IOTA ring construction is started. Its operation with electrons is expected in 2017. The concept of the OSC test in IOTA is getting matured. The beam optics is close to be finalized. It still has potential for further optimization. In particular, an increase of the beam dynamic aperture is desirable. Suppression of dispersion effects in the e.-m. wave focusing is our next high priority task. We expect to finish the conceptual design within one year.

Acknowledgements: The authors would like to express their gratitude to M. Andorf, P. Piot and J. Ruan.

REFERENCES

[1] S. van der Meer, Rev. Mod. Phys. 57, 689 (1985)
[2] D. Mohl, Stochastic cooling, in CERN Accelerator School, Fifth Advanced Accelerator Physics Course, ed. by S. Turner (CERN, Geneva, 1995), pp. 587–671.
[3]. J. Bisognano, C. Leemann, Stochastic cooling, in Summer School on High Energy Particle Accelerators, AIP Conference Proceedings 87, ed. by R.A. Carrigan et al. (American Institute of Physics, Melville, NY, 1982), pp. 584–655
[4] V. Lebedev, V. Shiltsev, "Beam Physics at Tevatron Collider", Springer, 2014.
[5] M. S. Zolotorev and A. A Zholents, Phys. Rev. E, **50**, 4, p. 3087 (1994).
[6] V. Lebedev, Yu. Tokpanov and M. Zolotorev, PAC'13, p. 422-424 (2013).
[7] V. Lebedev, "Optical Stochastic Cooling" in ICFA Beam Dynamics Newsletter, **No. 65**, p. 100 (2014), http://icfa-usa.jlab.org/archive/newsletter/icfa_bd_nl_65.pdf
[8] S. Nagaitsev, *et. al.*, p.16, IPAC-2012, (2012).
[9] G. Stancari, *et. al.*,, "Electron Lenses and Cooling for the Fermilab Integrable Optics Test Accelerator,", this conference.
[10] M. Andorf, *et. al.*, "Single pass amplifier for Optical Stochastic cooling proof-of-principle experiment at IOTA", this conference.

ISBN 978-3-95450-174-8